Integrated core transport modeling of NSTX plasmas

G. Avdeeva[1], D.J. Battaglia[2], W. Guttenfelder[2], S.M. Kaye[2],
J. McClenaghan[3], O. Meneghini[3], T. Odstrcil[3], S.P. Smith[3], K.E. Thome[3]
[1] *Oak Ridge Associated Universities, P.O. Box 117 Oak Ridge, TN, USA*
[2] *Princeton Plasma Physics Laboratory, 100 Stellarator Rd, Princeton, NJ 08540, USA*
[3] *General Atomics, PO Box 85608, San Diego, CA 92186–5608, USA*

Reliable numerical modeling of fusion plasmas is critical for understanding plasma behavior in current devices and to enable performance assessment and design of future fusion machines. Such modeling should combine different physics-based models into a consistent solution and allows straightforward validation against experimental data.

This work demonstrates the results of integrated modeling of low aspect ratio plasmas aiming to better understand what drives ion and electron heat transport in the core region of NSTX (National Spherical Torus Experiment) [1]. The presented illustrative example is a typical H-mode discharge #129017, which has been analysed in Ref. 2 and references therein. We focused on the time interval with low MHD activity at the middle of the current flattop where the main plasma parameters are: $I_p = 0.8\,MA$, $B_t = 0.45\,T$, $P_{\mathrm{NBI}} = 4.2\,MW$, $q_{95} = 9$, $\langle n_e \rangle = 6 \cdot 10^{19}\,m^{-3}$, $\beta_N = 4.4$, $\langle Z_{eff} \rangle = 1.25$.

The presented integrated modeling approach is based on the OMFIT integrated modeling framework [3], which provides a convenient interface for data preparation, numerical code execution, and theory/experiment comparison. Equilibrium reconstruction is an initial step for any plasma transport analysis. A self-consistent full kinetic equilibrium reconstruction can be obtained through several iterations of a cyclic workflow that includes producing an initial equilibrium reconstruction from available diagnostics, mapping experimental measurements onto flux space, and running transport codes to provide more accurate constraints of internal pressure and current density profiles. Based on NSTX specific diagnostic measurements, the initial equilibrium is constrained by magnetic, motional stark effect (MSE) and electron profiles measurements. Since NSTX has full radial coverage from the low field side (LFS) to the high field side (HFS) for the Thomson scattering (TS) diagnostic [4] and given the assumption of fast parallel heat conductivity, it is possible to apply isothermal constraints in the equilibrium reconstruction, where electron temperature measurements at two different radii (one LFS, one HFS) are constrained to be at the same flux surface. As seen in Fig. 1 (a) the equilibrium reconstruction with isothermal constraints provides an overlap of LFS and HFS experimental measurements mapped onto flux space. The isothermal constraint reconstruction has a shift in

the position of the last closed flux surface (LCFS) of around 2 cm inward on the LFS compared to the equilibrium where such constraints are not included.

This procedure of obtaining an equilibrium is similar to that explained in Ref.5; however, OMFIT allows users more options to preview and modify the weights of the constraints as well as tools for validation of the solution, which will be described below. Furthermore, OMFIT is integrated with the plasma transport code TRANSP [6; 7], which is necessary for estimating the fast ion pressure contribution to the total plasma pressure and for computing the plasma current density profile, including the bootstrap and beam driven currents. This information provides more accurate constraints on the internal plasma profiles for the next iteration of equilibrium reconstruction. For the selected neutral beam injection (NBI) heated shot, the contribution of the fast-ion to the total pressure is around 60% at the core and 10% at the edge (Fig. 1 (b)). The plasma current constraints are constructed so that the core is based on the MSE measurements. At the edge ($0.6 < \rho < 1$), where MSE measurements have a larger uncertainty, constraints are based on the TRANSP calculations of the edge current, where the bootstrap current has the largest contribution. The equilibrium reconstructions obtained in the initial iteration (Iteration 0) and after the first TRANSP calculations (Iteration 1) are shown on Fig. 1 (c-e). We can see that the plasma profiles determined with these TRANSP-based constraints are more peaked than in iteration 0. Changes in the magnetic equilibrium affect the mapping of the kinetic measurements, as well as the calculation of the deposition of the sources in the transport code and the bootstrap current. Remapping of experimental profiles into the new equilibria will affect the pressure and current profiles computed by TRANSP on the next iteration. As seen from Fig. 1 (c-e), the self-consistent solution for the case shown is obtained after iteration #2 and further iterations will not significantly change the solution.

Comparison of the experimental measurements with EFIT and TRANSP calculations is used as a validation metric for the solution. In Fig. 1 (f-g), a good agreement is observed between: the MSE measurements and the EFIT reconstruction; the measured neutron rate and that computed by TRANSP.

From the TRANSP simulations we found that the electron heat flux is much larger than the ion heat flux and therefore it is a dominant channel for heat loss. The electron-ion heat exchange term is of the same order of magnitude as the ion heat flux at the range $\rho \sim 0.5 - 0.7$. These power balance fluxes are used as input for the single-time-point TGYRO solver [8], which estimates the contributions of the turbulent and neoclassical transport to the total heat flux and to predict the temperature profiles. TGYRO predicts profiles by adjusting profile gradients until the total predicted fluxes from TGLF [9] and NEO [10] match the power balance fluxes, includ-

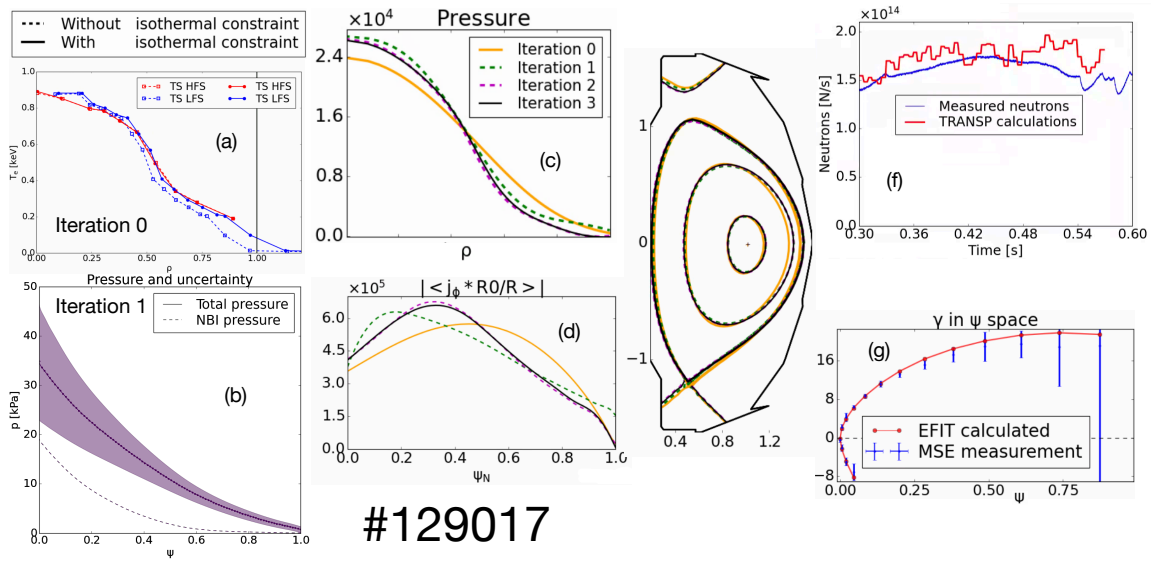

Figure 1: *(a) TS measurements mapped onto flux space obtained with and without isothermal constraints. (b) NBI pressure and total pressure with uncertainty. (c),(d),(e) Plasma pressure, current density profiles, and flux surface topology reconstructed on different iterations, (f) comparison of the measured neutron rate with TRANSP calculations, (d) comparison of the MSE measurements and the EFIT reconstruction*

ing a dynamic collisional exchange term based on the current electron and ion temperatures. TGLF provides quasi-linear turbulent fluxes estimated based on the profiles gradients. NEO is a neoclassical model that provides the contribution of neoclassical fluxes.

As seen from Fig. 2 the electron heat flux is completely turbulent and the ion heat flux is fully neoclassical. This result is in agreement with previous transport analyses of spherical tokamak plasmas [11]. As seen from Fig. 2 the experimental profiles are reasonably well reproduced by TGLF (with SAT1 [12], which takes into account effects of multi-scale turbulence) on the range $\rho \sim 0.4 - 0.7$; therefore, we can conclude that electrostatic drift wave turbulence plays the dominant role in turbulent electron heat transport in this plasma. This is confirmed by previous gyrokinetic simulations, which showed a small contribution of microtearing modes even though this is a high beta plasma [13]. In analysis presented here, the heat fluxes were evolved separately (holding T_e fixed when evolving T_i, and vice versa). We confirmed that moving the boundary conditions to ρ - 0.8 did not change the results of TGYRO prediction.

Future analysis will include a broader selection of NSTX shots for validation of the reduced turbulent transport model TGLF on the low aspect ratio plasma, and will attempt to predict more transport channels simultaneously.

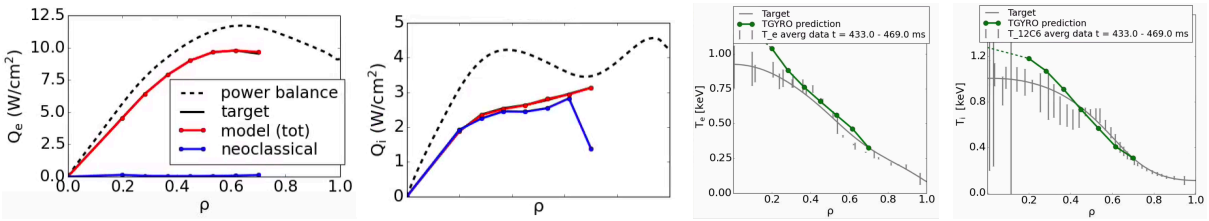

Figure 2: *Heat fluxes and plasma profiles predicted by TGYRO and compared with power balance TRANSP calculations and experimental measurements correspondingly.*

References

[1] S.M. Kaye et al., 2015 Nucl. Fusion **55** 104002.

[2] R. Maingi et. al., Nucl. Fusion **52** (2012) 083001

[3] O. Meneghini et al., Nuclear Fusion **55** (2015)

[4] B.P. LeBlanc et al., Review of Scientific Instruments **74**, 1659 (2003)

[5] S.A. Sabbagh et al., Nucl. Fusion **46** (2006)

[6] J Breslau et al., Computer Software. USDOE Office of Science (SC), FES (SC-24). (2018)

[7] B.A. Grierson et al., Fusion Sci. Technol.

[8] J. Candy, et. al., Phys. Plasmas **16** (2009)

[9] G.M. Staebler et. al., Phys. Plasmas (2005)

[10] E.A. Belli J. Candy, Plasma Phys. Control. Fusion (2008)

[11] S.M. Kaye et al., Nucl. Fusion **53** (2013)

[12] G.M. Staebler et. al., Physics of Plasmas **23** (2016)

[13] W. Guttenfelder et al., Nucl. Fusion **53** (2013)

Acknowledgement

This material is based upon work supported by the U.S. Department of Energy, Office of Science, Office of Fusion Energy Sciences under Awards DE-SC0021113 and DE-AC02-09CH11466.

Disclaimer